IVYSPRING INTERNATIONAL PUBLISHER

Theranostics

2020; 10(6): 2453-2462. doi: 10.7150/thno.42981

Research Paper

Tumor pH-responsive metastable-phase manganese sulfide nanotheranostics for traceable hydrogen sulfide gas therapy primed chemodynamic therapy

Ting He[1,2‡], Xialing Qin[1‡], Chao Jiang[1], Dawei Jiang[1], Shan Lei[1], Jing Lin[1], Wei-Guo Zhu[3], Junle Qu[2], Peng Huang[1✉]

1. Marshall Laboratory of Biomedical Engineering, International Cancer Center, Laboratory of Evolutionary Theranostics (LET), School of Biomedical Engineering, Shenzhen University Health Science Center, Shenzhen 518060, China.
2. Key Laboratory of Optoelectronic Devices and Systems of Ministry of Education and Guangdong Province, College of Optoelectronic Engineering, Shenzhen University, Shenzhen 518060, China.
3. Guangdong Key Laboratory of Genome Instability and Human Disease Prevention, Carson International Cancer Center, Department of Biochemistry and Molecular Biology, Shenzhen.

University School of Medicine, Shenzhen 518055, China.

‡ These authors contributed equally to this work.

✉ Corresponding author: Peng Huang. 1066 Xueyuan Boulevard, Shenzhen University Health Science Center, Shenzhen, 51860, China. E-mail: peng.huang@szu.edu.cn.

Received: 2019.12.12; Accepted: 2019.12.24; Published: 2020.01.20

Abstract

Manganese-based nanomaterials have piqued great interest in cancer nanotheranostics, owing to their excellent physicochemical properties. Here we report a facile wet-chemical synthesis of size-controllable, biodegradable, and metastable γ-phase manganese sulfide nanotheranostics, which is employed for tumor pH-responsive traceable gas therapy primed chemodynamic therapy (CDT), using bovine serum albumin (BSA) as a biological template (The final product was denoted as MnS@BSA). The as-prepared MnS@BSA can be degraded in response to the mildly acidic tumor microenvironment, releasing hydrogen sulfide (H_2S) for gas therapy and manganese ions for magnetic resonance imaging (MRI) and CDT. *In vitro* experiments validated the pH-responsiveness of MnS@BSA at pH 6.8 and both H_2S gas and •OH radicals were detected during its degradation. *In vivo* experiments showed efficiently tumor turn-on T_1-weighted MRI, significantly suppressed tumor growth and greatly prolonged survival of tumor-bearing mice following intravenous administration of MnS@BSA. Our findings indicated that MnS@BSA nanotheranostics hold great potential for traceable H_2S gas therapy primed CDT of cancer.

Key words: manganese sulfide, hydrogen sulfide, gas therapy, chemodynamic therapy, nanotheranostics.

Introduction

Cancer nanotheranostics provide a new solution for cancer management using nanotechnology to integrate medical imaging and therapy of cancer [1-7]. Magnetic resonance imaging (MRI) is a classical noninvasive medical imaging that benefits high spatial resolution without ionizing radiation and tissue depth limits, which is widely employed in MRI-based nanotheranostics [8-12]. For example, Gadolinium (Gd)-nanomaterials and iron oxide nanoparticles have been developed for longitudinal (T_1) and transverse (T_2) MR contrast agents, respectively [13-18]. Recently, manganese-based MR contrast agents, such as manganese sulfide (MnS) [19-21], manganese oxide [22], manganese dioxide [23-27], manganese carbonate [28], and manganese iron [29-30], have been widely explored in the field of cancer

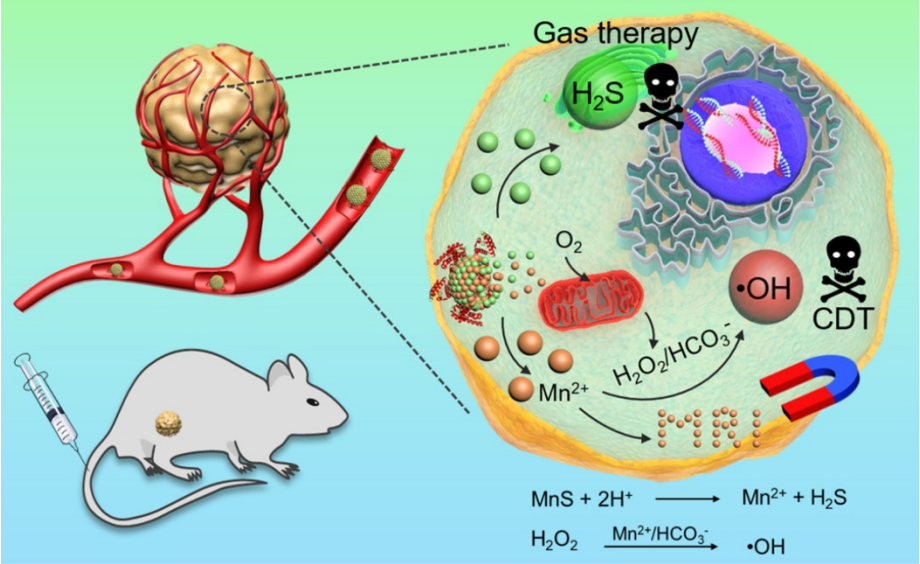

Scheme 1. Metastable-phase manganese sulfide nanotheranostics (MnS@BSA) for tumor pH-responsive traceable hydrogen sulfide (H_2S) gas therapy primed chemodynamic therapy (CDT) of cancer. The MnS@BSA can be degraded in response to the mildly acidic tumor microenvironment, releasing H_2S for gas therapy and Mn^{2+} for magnetic resonance imaging (MRI) and CDT of cancer.

theranostics. The MnS are mainly included three crystal formations: α-phase, β-phase and γ-phase. The α-phase MnS is highly stable and non-degradable, raising the potential long-term toxicity that hampers its further biomedical application [31-32]. On the contrary, γ-MnS is metastable and can be degraded in the acidic microenvironment and release manganese ions (Mn^{2+}). Therefore, the development of γ-MnS-based nanotheranostics is promising for tumor pH-responsive T_1-weighted MRI of cancer.

For cancer therapy, chemodynamic therapy (CDT) can convert hydrogen peroxide (H_2O_2) into the toxic hydroxyl radical (•OH) at tumor tissues, thus killing tumor cells [33-35]. Recently, it has been reported MnO_2 shell was decomposed in tumor microenvironment to release Mn^{2+}, which can catalyze H_2O_2 to produce •OH at the presence of HCO_3^- in physiological environments by a Fenton-like reaction manner as that catalyzed by iron ions [36]. This process consumes glutathione (GSH) and enhances CDT effect simultaneously. Therefore, we proposed the released Mn^{2+} from tumor pH-responsive γ-MnS nanoparticles could be also used for CDT of cancer.

Additionally, gas therapy is an emerging therapeutic strategy based on the bioeffects of several kinds of gases, such as nitric oxide (NO), carbon monoxide (CO), hydrogen sulfide (H_2S) and hydrogen (H_2) [37-39]. H_2S gas is an important endogenous bio-signaling molecule, similar to NO and CO [38, 40-42],and exhibits concentration-dependent biological effects [43-44]. It can be metabolized in mitochondria at nanomolar (nM) concentrations, while at micromolar (μM) concentrations, H_2S gas shows a substantial anti-proliferative effect on MCF-7 breast cancer cells [45]. The anticancer effect of H_2S gas has also been reported in living organisms [45-46]. However, traditional H_2S donors, such as Na_2S and NaHS, the H_2S gas release is too fast to maintain a long-term effect, while organic compounds, such as GYY4137, are too complicated to obtain [46]. Therefore, the development of novel H_2S donors is highly desirable for cancer gas therapy.

The combination of CDT and H_2S gas therapy into a single nanoplatform can achieve enhanced anticancer effect. Because H_2S gas is a signal molecule that, like NO gas, can cause vasodilation and reduce vascular tension in solid tumors. Herein, we developed a facile wet-chemical method to synthesize size-controllable, biodegradable, and metastable γ-phase MnS using bovine serum albumin (BSA) as a template for tumor pH-responsive T_1-weighted MRI guided the integration of CDT and gas therapy (**Scheme 1**). BSA is used to regulate the size of MnS nanoparticles by tuning the ratio of BSA and Mn^{2+}. The as-prepared MnS@BSA is tumor pH-responsive and will be dissociated in acidic tumor microenvironment, producing H_2S gas and releasing Mn^{2+} ions simultaneously. The former can be used for gas therapy while the latter can provide CDT and serve as a contrast agent for T_1-weighted MRI.

Experimental Section

Synthesis of MnS@BSA

MnS@BSA were synthesized by gradually adding $Mn(NO_3)_2$ to a Na_2S solution. Typically, different amounts of BSA (2.5, 5, and 10 mg) was added into 400 μL of Na_2S (0.5 M). The volume was

later set to 40 mL using deionized water and pH was adjusted to 7.4-7.8 using 0.5 M H_2SO_4. After 5 min of vacuuming to remove O_2, the system was protected by N_2. Then 2 mL of $Mn(NO_3)_2$ (0.05 M) was added to the mixed solution by a micro-injection pump in 30 min. A flesh pink product was produced, washed and concentrated by centrifugation (12000 rpm, 30 min). The obtained nanoparticles were named as MnS@BSA-2.5, MnS@BSA-5 and MnS@BSA-10. The MnS@BSA-10 with uniform size was used for further studies.

Levels of Mn^{2+} and H_2S Released from MnS@BSA

For Mn^{2+}, 400 μL of MnS@BSA (5.5 mM) was added into a 3500 Da dialysis bag with PBS buffer (50 mL 10 mM) at pH 6.8 and 7.4, respectively. The solutions were kept stirring at 37 °C and 2 mL was removed for analysis at 0, 0.5, 1, 2, 4, 8, 12, 24, 48, and 72 h. Mn element quantification was performed by using an ICP-AES. For H_2S, 400 μL of MnS@BSA (5.5 mM) was added into a 3500 Da dialysis bag with HEPES buffer (50 mL 10 mM) at pH 6.8 and 7.4, respectively. 1 mL of the solution was removed as a working solution for H_2S analysis at 0, 1, 2, 5, 10, 20, 30, 60 min. H_2S concentration was analyzed using a standard MB method[43]. Briefly, 100 μL of the working solution, 100 μL of 1% (w/v) $Zn(OAc)_2$, 20 μL of DMPD (20 mM) and 20 μL of $FeCl_3$ (30 mM) were mixed, kept at room temperature for 15-20 minutes, and the optical density (OD) at 663 nm was measured.

Hydroxyl Radical Catalyzed by MnS@BSA

MnS@BSA or $MnCl_2$ was added into 10 μg/mL MB solution which containing 25 mM $NaHCO_3$ and 10 mM H_2O_2. The OD@665 nm of the above mixture solution was monitored by UV-Vis spectrophotometer at different time points from 0 to 60 min. For ESR detection, 25 mM of $NaHCO_3$ were used as the solvent for H_2O_2 (10 mM) and DMPO (100 μM). Five groups were tested: H_2O_2, MnS@BSA, $MnCl_2$, H_2O_2 + MnS@BSA, and H_2O_2 + $MnCl_2$. The concentrations of $MnCl_2$ and MnS@BSAwere set to 5 μM and the total volume was 0.5 mL. All reagents were mixed and kept for 30 min before hydroxyl radicals were measured.

In vitro Combination Therapy

MCF10A and 4T1 cells were seeded into 96-well plates at a density of 5000 cells per well. After 12 h in the incubator, the cells were incubated with MnS@BSA, $MnCl_2$, Na_2S ([Mn]/[S] = 0-200 μM) for 24 h. To assess the cytotoxicity of MnS@BSA, various concentrations of antioxidant lascorbic acid (AA, 0-80 μM) in 10 μM with different concentration of MnS@BSA ([Mn]=0-200 μM) were tested. The standard MTT assay was carried out to evaluate the cell viability.

Hydroxyl Radicals and H_2S in Cells

5×10^5 of 4T1 cancer cells were digested and resuspended into 2 mL of DMEM and subcultured into φ15 confocal laser scanning microscopy (CLSM)-exclusive culture disks for another 12 h. Subsequently, the medium was removed and the disks were rinsed by PBS twice before adding 1 mL of DMEM containing 50- 200 μM of MnS@BSA, 200 μM of $MnCl_2$. Finally, the medium was removed and the fluorescence probe addition: 25 μM of non-fluorescent DCFH-DA was added to reduce hydroxyl radical for 30 min, then the fluorescence of DCF was observed on CLSM. For H_2S, 2.5×10^5 4T1 cancer cells were subcultured into 24-well plates for 12 h. After incubated with 100 μM of the WPS-5 probe for 30 min, then treated with 0, 50, 100, 200 μM of MnS@BSA and 200 μM of Na_2S. Then added HEPES containing 100 μM of CTAB (pH 7.4,). After 10 min, fluorescence images were acquired.

In vivo Imaging and Biodistribution

Tumor-bearing mice were scanned with a 3T clinical United Imaging 790 MRI scanner (United Imaging, Shanghai, China) before and after intravenous administration of 2.5 mg/kg of Mn (MnS@BSA or $MnCl_2$). T_1-weighted images were acquired by FSE sequence at 0, 1,2, 4, 8, and 24 h and the following parameters were applied: TR=700 ms, TE=14.3 ms, Flip Angle=145 °, matrix size, 160 x 160, slice thickness, 1.5 mm. Signal intensities were measured in defined regions of interest (ROIs) with software named Image J. MRI were performed at 0, 1, 2, 4, 8, 24 h post-injection.

Six tumor-bearing mice were divided into two groups (n=3). After administration of 2.5 mg/kg of MnS@BSA through their tail veins. One group was euthanized after 4 hours, and the other was euthanized after 24 hours. Tumors and major organs (heart, liver, spleen, lung, kidney and muscle) were obtained and washed with PBS. Each organ was immersed in 3 mL of nitric acid overnight, and then heated to 150 °C. The final volume was set to 1.5 mL. The concentration of Mn was measured by ICP-AES to estimate the *in vivo* bio-distribution of MnS@BSA.

In vivo Combination Therapy

The therapeutic effects of MnS@BSA were examined on 4T1-Luciferase mammary tumor xenograft on BALB/c mice. Tumor-bearing mice were randomly divided into seven groups: 5 mice per group, administered dose was 2.5 mg/kg MnS@BSA. The seven groups were: PBS, $MnCl_2$, Na_2S, MnS@BSA -2.5, MnS@BSA -5, MnS@BSA -10 and MnS@BSA -10+AA. Their body weights and tumor volumes were

measured every two days to evaluate the therapeutic performance. FL imaging of mice were recorded on day 2, 4, 6, 8 and 14 post-treatments. Before FL imaging, 15 mg/mL of D-luciferase potassium salt was intraperitoneally injected at a dose of 10 μL/g, and bioluminescence imaging was performed at 10-15 min post-injection for tumor growth evaluation.

Results and Discussions

Preparation and Characterization of MnS@BSA

The α-MnS was commonly synthesized by the high temperature decomposition of manganese oleate in oil phase [19, 47-48]. It was not water-soluble and needed further surface modification for biomedical applications. In our case, MnS@BSA was synthesized by a wet-chemical method (**Figure 1A**). Briefly, manganese source ($MnCl_2$) was slowly added to a mixture solution of Na_2S and BSA, which was vacuumed and protected with N_2 gas to obtain a pink solution (**Figure S1**), the typical color of γ-phase MnS. XRD pattern (JCPDS Card No.40-1289) further confirmed that MnS@BSA is γ-phase MnS (**Figure 1B**). As shown in **Figure 1C,** MnS@BSA exhibited well-defined sphere. The size of MnS@BSA can be controlled from 300 to 150 nm by adjusting the amount of BSA from 2.5 to 10 mg. More BSA were added, the size of MnS@BSA were smaller (**Figure S2**). The MnS@BSA (10 mg of BSA) with the smallest size (~ 150 nm) was selected for the following experiments. As shown in the element mapping of MnS@BSA (**Figure 1D**), C, N and O elements were assigned to BSA, S and Mn elements were assigned to MnS. These results indicated that γ-phase MnS was successfully synthesized using BSA as template, which can improve its solubility and biocompatibility.

Hydroxyl Radicals and H_2S of MnS@BSA

The as-synthesized MnS@BSA can be easily decomposed and oxidized in aqueous solutions containing oxygen, especially under acidic conditions. As shown in **Figure 2A** and **2B**, MnS@BSA was degraded much faster in the acidic solution than in

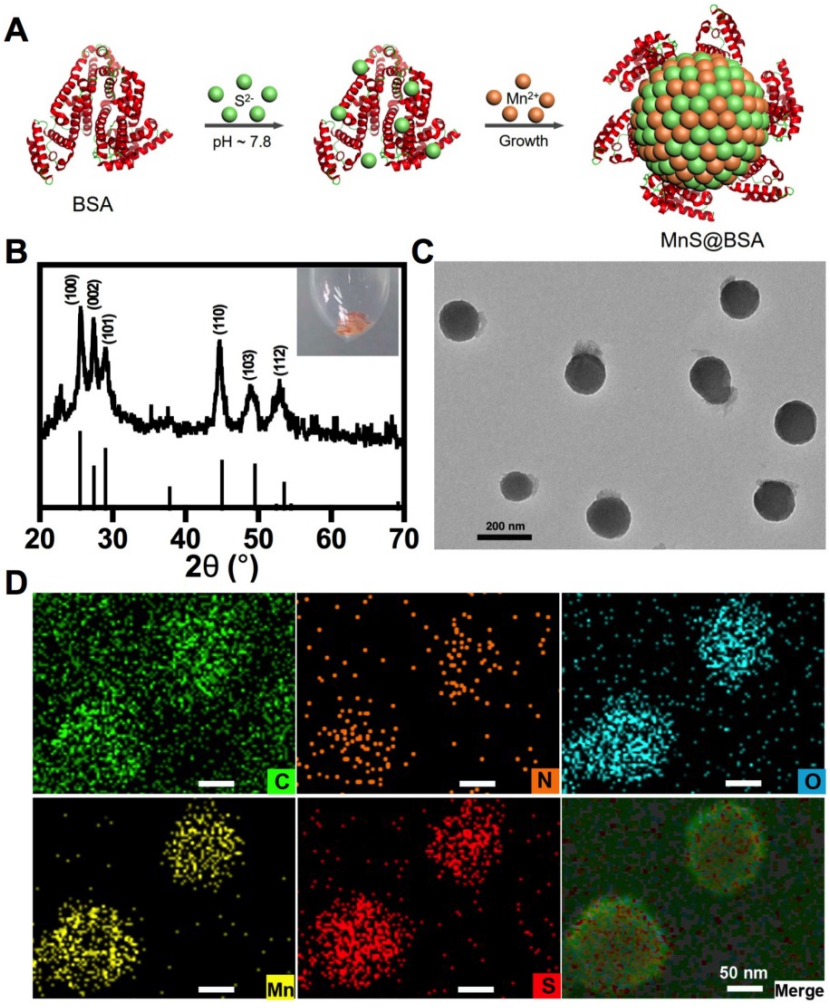

Figure 1. (A) The schematic illustration of the synthesis of metastable phase MnS@BSA. MnS@BSA (B) XRD pattern of MnS@BSA, (C) TEM image of MnS@BSA, scale bar 200 nm, (D) Element mapping images of MnS@BSA. Scale bar 50 nm.

the neutral solution. These results are consistent with the levels of Mn^{2+} released from MnS@BSA in PBS buffer at different pH values (**Figure 2C**). After 8 h, 98.3% of MnS@BSA was degraded in acidic solution, while only 57.3% of Mn^{2+} was released at pH 7.4. Afterwards, the degradation of MnS@BSA in 4T1 cells was observed using bio-TEM imaging at 8 and 24 h post-incubation (**Figure S3**). A lot of MnS@BSA were observed inside 4T1 cells after 2 h incubation. After 24 h incubation, sphere MnS@BSA were hardly found in 4T1 cells. These results indicated that MnS@BSA could be degraded in 4T1 cells gradually. Meanwhile, the concentration of released H_2S from MnS@BSA under different pH conditions was measured using the methylene blue (MB) method. The H_2S gas from MnS@BSA was released much faster in the acidic solution than in the neutral solution (**Figure 2D**). The concentration of H_2S can reach up to 12 μM, which is able to kill cancer cells efficiently. These results suggested that pH-responsive MnS@BSA could be fully degraded in aqueous solutions at pH 6.8, followed by the release of Mn^{2+} and H_2S gas, which promises for cancer diagnosis and treatment.

Manganese element is a trace element in living organisms, which may catalyze Fenton-like reactions in physiological environment to produce highly toxic •OH radicals [36]. The Mn^{2+} and HCO_3^- in the blood constitute the catalysts for Fenton reactions, which can consume enriched H_2O_2 in tumor microenvironments to generate •OH radials. In order to evaluate the Fenton-like reactivity of MnS@BSA, MnS@BSA was added into MB solution containing HCO_3^- and H_2O_2, as shown in **Figure 2E**. The degradation of MB indicated the concentration dependency of manganese concentrations. Both $MnCl_2$ (used as a control) and MnS@BSA produced •OH that could degrade MB at a similar rate (**Figure S4**). A unique quadruple peak of •OH was observed in electron spin resonance (ESR) spectra (**Figure 2F**), but was not observed in control groups. All results indicated that released Mn^{2+} ions from MnS@BSA can generate a lot of •OH under physiological conditions.

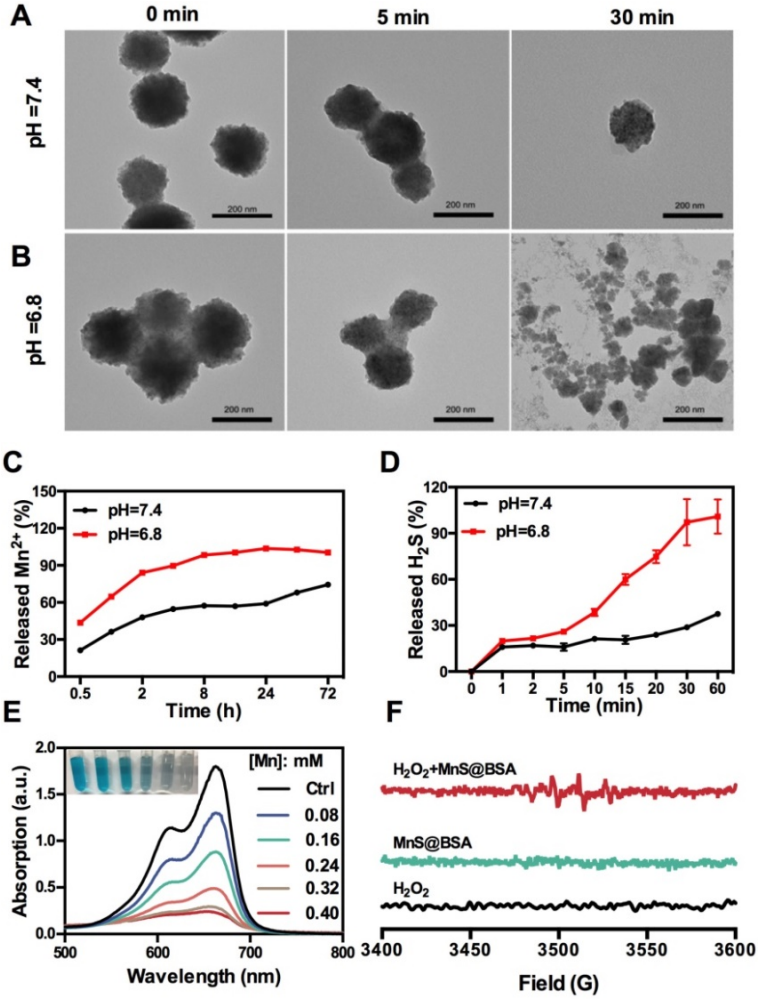

Figure 2. TEM images of MnS@BSA at 0, 5, and 30 min after incubation in HEPES buffer at pH=7.4 (A) and pH= 6.8 (B). (C) Levels of Mn^{2+} released from MnS@BSA in PBS buffer. (D) Levels of H_2S gas released from MnS@BSA at HEPES buffer of pH=7.4 and pH=6.8 with N_2 protection. (E) UV-Vis absorption spectra and photographs of methylene blue solutions after different amounts of MnS@BSA adding to H_2O_2 (9 mM)/$NaHCO_3$ (25 mM) solution for Mn^{2+} catalyzed Fenton-like reaction for 30 min. (F) ESR spectra of H_2O_2, MnS@BSA and MnS@BSA + H_2O_2 added in $NaHCO_3$ (25 mM) solution reacted for 2 h.

In vitro Combination Therapy

Next, *in vitro* experiments of MnS@BSA were performed to evaluate its combination cancer therapeutic effect and cytotoxicity. As shown in **Figure 3A**, cell viability showed a concentration-dependent therapeutic effect on 4T1 cells when incubated with Na_2S, $MnCl_2$ and MnS@BSA (10-200 μM), which is in agreement with the live/dead cell staining results (**Figure S5**). The therapeutic effect of MnS@BSA on tumor cells can be attributed to the bioeffects of both H_2S gas and •OH radicals. The mortality of 4T1 cells caused by H_2S gas and •OH radicals was calculated in **Figure 3B**. As one can see that 65-69% of cytotoxicity was induced by •OH radicals, which suggested •OH radicals were more potent than H_2S gas at all tested concentrations. Interestingly, Na_2S, $MnCl_2$ and MnS@BSA showed negligible cytotoxicity on MCF10A cells (a control cell line) as evidenced by the maintained cell viability at ~75% at all tested concentrations (10-200 μM) (**Figure S6**). The different cytotoxicity between 4T1 and MCF10A cells was attributed to the levels of H_2O_2 inside cells. Indeed, the H_2O_2 concentration of 4T1 cells was 2.2 times higher than that of MCF10A (**Figure 3C**), followed by HeLa and A375 cells. This higher concentration of H_2O_2 allowed for the enhanced •OH generation for responsive CDT treatment of 4T1 cells but no other cell lines. Therefore, MnS@BSA elicited an improved therapeutic effect on tumor cells with high levels of H_2O_2. To further demonstrate the therapeutic mechanism, reductive L-ascorbic acid (AA) was used to neutralize •OH radicals at cell level. By adding 10 μM of AA to different concentrations of $MnCl_2$ (**Figure 3D**) or MnS@BSA (**Figure 3E**), 4T1 cell viability could increase by 10-21%. In particular, with the increase of AA, toxic effects of •OH radicals produced by MnS@BSA were gradually decreased (**Figure 3F**). These results indicated that therapeutic effects of MnS@BSA were attributed to the combination effects of •OH radicals and H_2S gas.

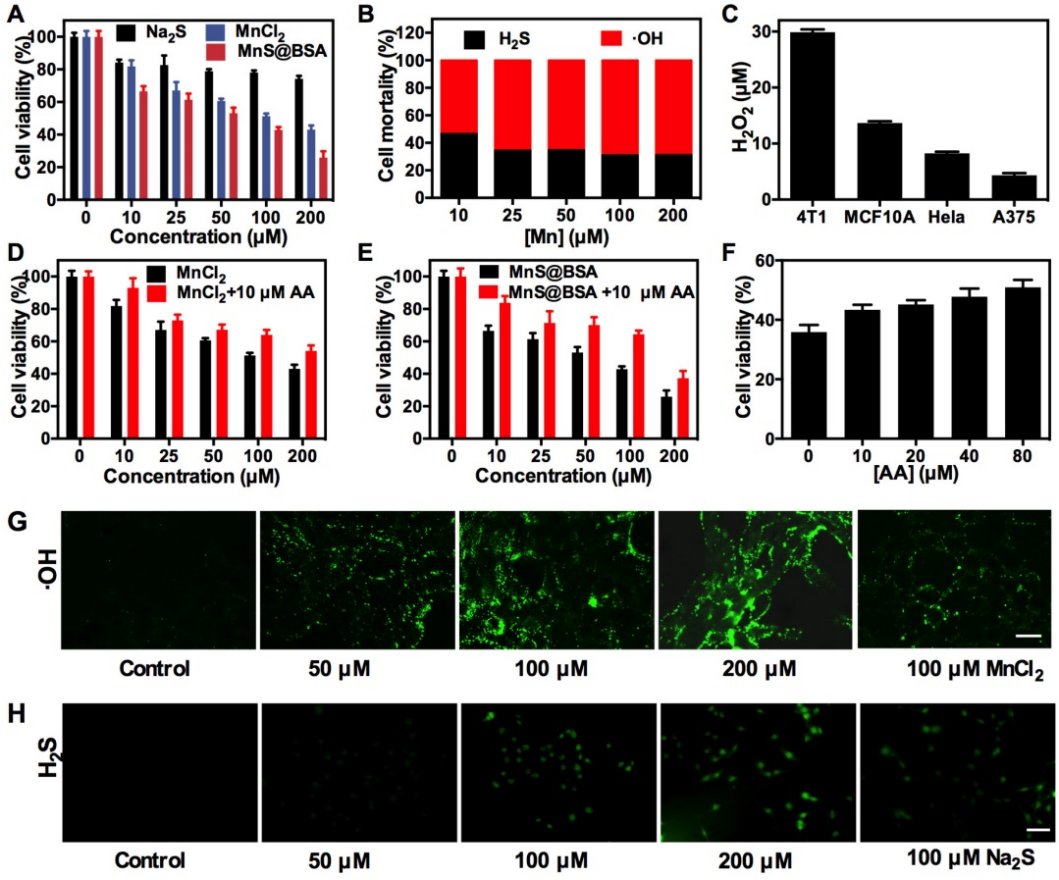

Figure 3. (A) Cell viability of 4T1 cells after incubation with Na_2S, $MnCl_2$ and MnS@BSA at different concentrations for 24 h. (B) Mortality of 4T1 cells caused by •OH radicals and H_2S gas after incubated with MnS@BSA for 24 h. (C) H_2O_2 concentrations in 4T1, MCF10A, HeLa, A375 cells detected by a H_2O_2 kit. Viability of 4T1 cells incubated with (D) $MnCl_2$, $MnCl_2$+10 μM L-ascorbic acid (AA), (E) MnS@BSA, MnS@BSA+10 μM AA. (F) Cytotoxicity of 4T1 cells incubated with 200 μM of MnS@BSA and various concentrations of AA: 0. 10, 20, 40, 80 μM for 24 h. (G) Confocal images of 4T1 cells incubated with various concentration of MnS@BSA: 0, 50, 100, 200 μM and $MnCl_2$: 100 μM for 4 h and stained with DCFH-DA fluorescence probe. (H) Fluorescence images of 4T1 cells incubated with WSP-5 H_2S fluorescence probe for 30 min, subsequently adding various concentration of MnS@BSA :0, 50, 100, 200 μM and Na_2S 100 μM for 30 min, scale bar 100 μm.

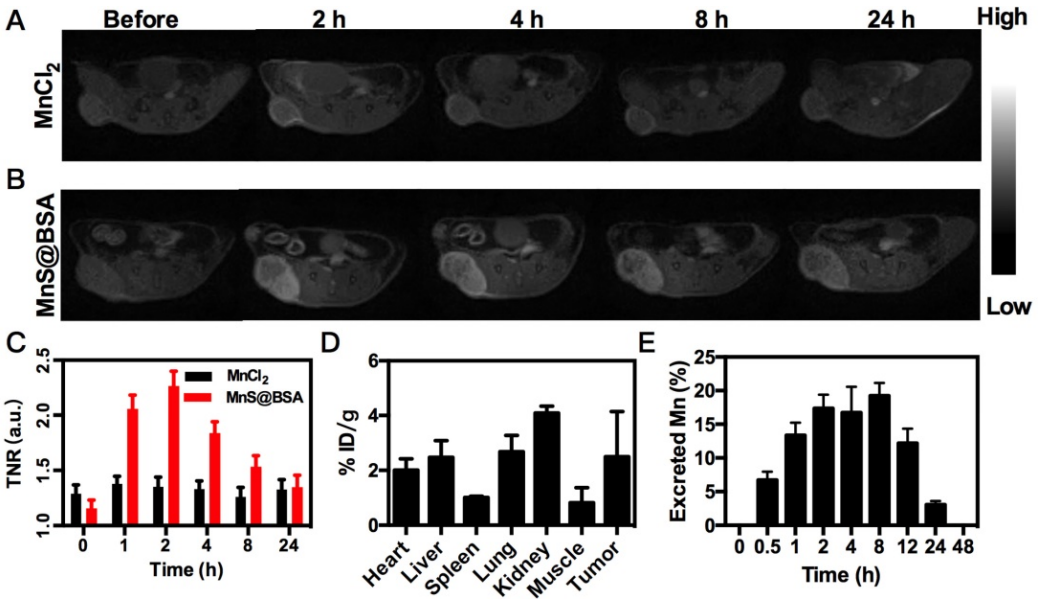

Figure 4. MRI images of 4T1 tumor-bearing mice after i.v. injection of $MnCl_2$ (A), MnS@BSA (B) at various time points. (C) The TNR contrast ratio after i.v. injection of MnS@BSA or $MnCl_2$. (D) Biodistribution of manganese element after injection of MnS@BSA at 24 h post-injection. (E) The content of manganese element in mice excrements after injection of MnS@BSA over time.

In order to directly observe the generation of •OH radicals *in vitro*, 4T1 cells were incubated with different concentrations of MnS@BSA for 4 h. Then the probe of oxidative stress, 2′,7′-dichlorofluorescin diacetate (DCFH-DA), was added. After deacetylates with intracellular esterase to form the non-fluorescent 2′,7′-dichlorofluorescin (DCFH), DCFH would be further oxidized into bright green fluorescent dye, 2′,7′-dichlorofluorescein (DCF) by reactive oxygen species (ROS) including •OH radicals [36, 49], which can be observed by confocal laser scanning microscopy (CLSM). As expected, the fluorescence intensity of DCF was elevated as the amount of MnS@BSA increased from 50 to 200 μM, which suggested the increase of oxidative stress strongly depended on the concentration of MnS@BSA (**Figure 3G**). These results are consistent with the results of Fenton-like reaction mentioned above. Similarly, free $MnCl_2$ also could induce the generation of ROS. Meanwhile, H_2S gas released in 4T1 cells was observed by adding a Washington State Probe-5 (WSP-5) H_2S fluorescent probe (**Figure 3H**). It is based on 2-pyridyl disulfide fluorescent, which release the fluorophores and turn on the fluorescence by tandem nucleophilic subsitution-cyclization reaction. WSP-5 probe can selectively and rapidly react with H_2S in cells to generate a green fluorescence signal [50]. The fluorescence intensity of WSP-5 was increased in accordance to the added concentration of MnS@BSA. The same effect was also evidenced in the Na_2S group, further indicating that MnS@BSA can release H_2S gas inside cells. All these results proved that MnS@BSA can generate •OH radicals and H_2S in 4T1 cells, promising for combined CDT and H_2S gas therapy.

In vivo Imaging and Biodistribution

The released Mn^{2+} ions from MnS@BSA are not only a catalyst for the Fenton-like reaction, but also a contrast agent for tumor pH-responsive T_1-weighted MRI. Since MnS@BSA is pH-responsive in acidic solutions, its longitudinal relaxivity (r_1) was measured under different pH conditions, as shown in **Figure S7**. The T_1 relaxivity of MnS@BSA, r_1, was calculated to be 23.67 $mM^{-1}s^{-1}$ in a pH 6.8 buffer at 2 h. Encouraged by the high r_1 value of MnS@BSA at pH 6.8, we performed *in vivo* tumor pH-responsive MRI of MnS@BSA on 4T1 tumor-bearing mice after intravenous (i.v.) injection with $MnCl_2$ as a control. Tumor signal of 4T1 bearing mice treated with MnS@BSA clearly increased over time, while the tumor signal kept no change for mice treated with $MnCl_2$ (**Figure 4A** and **B**). The tumor to normal ratio (TNR) of mice treated with MnS@BSA reached to a peak number of 2.26 at 2 h post-injection (**Figure 4C**). The mice treated with $MnCl_2$ showed negligible MR contrast enhancement. These results were further confirmed by the biodistribution study of Mn element at 4 h post-injection (**Figure 4D**). Since Mn^{2+} can be gradually excreted through metabolism, we also monitored Mn levels in excrements (**Figure 4E**). At 48 h post-injection, Mn concentration in mice was reduced to 0.02%, suggesting that MnS@BSA could be fully excreted within one day. These results suggested MnS@BSA could be fully cleared from the body of mice and exempt from the risk of potential long-term toxicity.

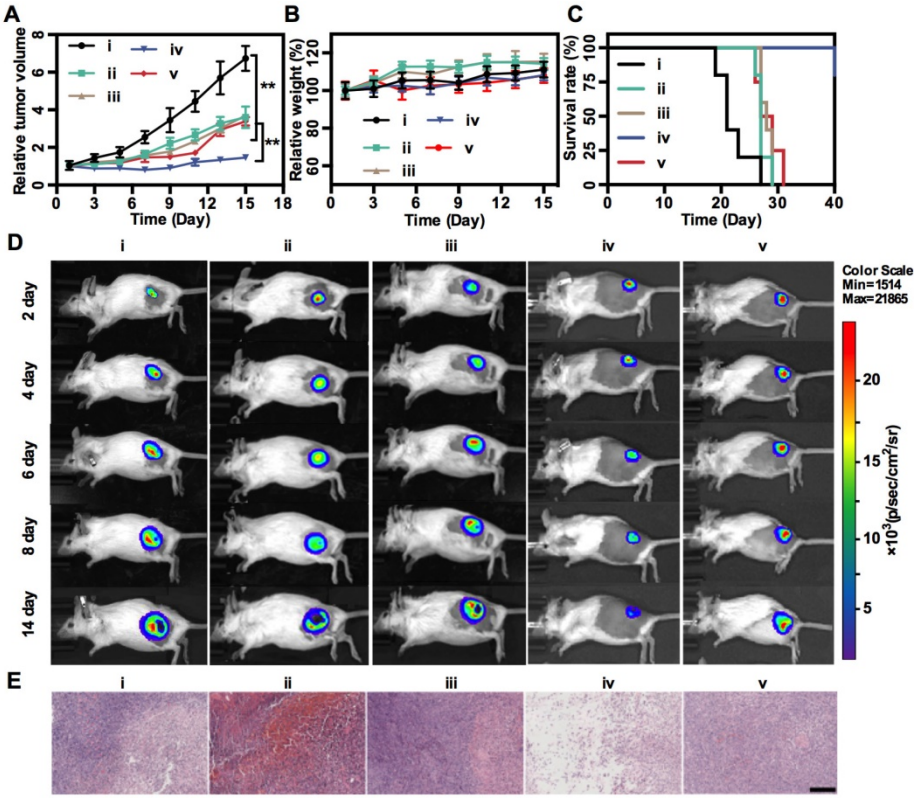

Figure 5. *In vivo* treatment. Tumor growth profiles (A), mice weight changes (B), and survival rates (C) of 4T1-luc tumor-bearing mice in different treatment groups: (i) Saline, (ii) $MnCl_2$, (iii) Na_2S, (iv) MnS@BSA, (v) MnS@BSA+AA. (D) *In vivo* bioluminescence images of 4T1-luc tumor-bearing mice in 5 groups throughout the treatment. (E) H&E staining images of tumors in all experiments groups. Scale bar: 200 μm, **p<0.05.

In vivo Combination Therapy

Finally, *in vivo* MnS@BSA-induced therapeutic effect was studied on 4T1-luc tumor-bearing mice. Mice were randomly divided into 5 groups: (i) saline, (ii) $MnCl_2$, (iii) Na_2S, (iv) MnS@BSA, (v) MnS@BSA+AA. The tumor volumes were monitored every 2 d during 2 weeks and normalized to their initial size in **Figure 5A**. The saline control group showed fast tumor growth, whereas the MnS@BSA treated group exhibited higher tumor suppression as compared with $MnCl_2$ and Na_2S treated group. The MnS@BSA+AA treated group exhibited obvious tumor regrowth after day 11, due to the neutralization of •OH radicals by AA. These results suggested the combination effect of CDT/gas therapy over any single modality treatment solely. For all groups, mice showed no noticeable body weight change, suggesting no systemic toxicity of MnS@BSA (**Figure 5B**). Meanwhile, the survival of mice administered with MnS@BSA was greatly prolonged (**Figure 5C**). More importantly, no obvious toxicity was induced by MnS@BSA, as evidenced by results of blood biochemistry, hematology analysis, and acute toxicity measurement of all major organs (**Figure S8-10**). Furthermore, all tumor growth was also monitored using bioluminescence imaging during treatment period. As shown in **Figure 5D,** the tumor luminescence was located on right hind of all groups in the whole treatment process. Especially, only the tumor of MnS@BSA group showed obviously suppression effect, but tumors of other groups kept growth. After different treatments, H&E staining images of all treatment groups were taken (**Figure 5E**). Tumors of saline, $MnCl_2$ and Na_2S groups show more chromatin and large nuclei, indicated silght effect of tumor cell proliferation. But for MnS@BSA treated group, the tumor slices shown that the chromatin was pyknotic or even absent in the slice. MnS@BSA-AA group can consume some ·OH to reduce the oxidative damage, which show more chromatin than MnS@BSA group. The tumors treated with CDT/gas combination therapy showed much higher damage than other groups.

Conclusions

In conclusion, we have developed a tumor pH-responsive metastable-phase MnS@BSA for combined CDT and H_2S gas therapy. The as-prepared metastable-phase MnS@BSA is able to response mildly acidic microenvironment and can release Mn^{2+} for Fenton-like reaction to generate •OH at the presence of endogenous H_2O_2 of tumor cells. The MnS@BSA can also generate H_2S to benefit gas

therapy of cancer. Furthermore, the size-controllable MnS NPs can be used as an MRI contrast agent for treatment monitoring owing to its high r_1 relaxivity of Mn^{2+} ions. This work provides a new design strategy of a nanotheranostic agent for traceable H_2S gas therapy ydrogen primed CDT. Our findings open new horizons for the biomedical applications of manganese-based cancer theranostics.

Acknowledgements

This work is financially supported by the National Key Research and Development Program (2018YFA0704003), the Guangdong Province Natural Science Foundation of Major Basic Research and Cultivation Project (2018B030308003), the Basic Research Program of Shenzhen (JCYJ20180 507182413022, JCYJ20170412111100742), the National Natural Science Foundation of China (31771036, 51703132), and the Fok Ying-Tong Education Foundation for Young Teachers in the Higher Education Institutions of China (161032). We thank Instrumental Analysis Center of Shenzhen University (Lihu Campus).

Supplementary Material

Supplementary figures and tables.
http://www.thno.org/v10p2453s1.pdf

Competing Interests

The authors have declared that no competing interest exists.

References

1. Fan W, Yung B, Huang P, Chen X. Nanotechnology for multimodal synergistic cancer therapy. Chem Rev. 2017; 117: 13566-638.
2. Park SM, Aalipour A, Vermesh O, Yu JH, Gambhir SS. Towards clinically translatable in vivo nanodiagnostics. Nat Rev Mater. 2017; 2: 17014.
3. Shi S, Kong N, Feng C, Shajii A, Bejgrowicz C, Tao W, et al. Drug Delivery Strategies for the Treatment of Metabolic Diseases. Advanced healthcare materials. 2019; 8: e1801655.
4. Chen H, Zhang W, Zhu G, Xie J, Chen X. Rethinking cancer nanotheranostics. Nat Rev Mater. 2017; 2: 17024.
5. Xie J, Lee S, Chen X. Nanoparticle-based theranostic agents. Adv Drug Deliv Rev. 2010; 62: 1064-79.
6. Zhang J, Ning L, Huang J, Zhang C, Pu K. Activatable molecular agents for cancer theranostics. Chemical Science. 2020: 10.1039/c9sc05460j.
7. Jiang Y, Huang J, Zhen X, Zeng Z, Li J, Xie C, et al. A generic approach towards afterglow luminescent nanoparticles for ultrasensitive in vivo imaging. Nat Commun. 2019; 10: 2064.
8. Lim EK, Huh YM, Yang J, Lee K, Suh JS, Haam S. pH-triggered drug-releasing magnetic nanoparticles for cancer therapy guided by molecular imaging by MRI. Adv Mater. 2011; 23: 2436-42.
9. Li B, Gu Z, Kurniawan N, Chen W, Xu ZP. Manganese-Based Layered Double Hydroxide Nanoparticles as a T1 -MRI Contrast Agent with Ultrasensitive pH Response and High Relaxivity. Adv Mater. 2017; 29: 8.
10. Kim T, Momin E, Choi J, Yuan K, Zaidi H, Kim J, et al. Mesoporous silica-coated hollow manganese oxide nanoparticles as positive T1 contrast agents for labeling and MRI tracking of adipose-derived mesenchymal stem cells. J Am Chem Soc. 2011; 133: 2955-61.
11. Wang Z, Zhang Y, Ju E, Liu Z, Cao F, Chen Z, et al. Biomimetic nanoflowers by self-assembly of nanozymes to induce intracellular oxidative damage against hypoxic tumors. Nat Commun. 2018; 9: 3334-48.
12. Zhang Y, Bo S, Feng T, Qin X, Wan Y, Jiang S, et al. A Versatile Theranostic Nanoemulsion for Architecture-Dependent Multimodal Imaging and Dually Augmented Photodynamic Therapy. Adv Mater. 2019; 31: e1806444.
13. Lin LS, Yang X, Zhou Z, Yang Z, Jacobson O, Liu Y, et al. Yolk-Shell Nanostructure: An Ideal Architecture to Achieve Harmonious Integration of Magnetic-Plasmonic Hybrid Theranostic Platform. Adv Mater. 2017; 29: 1606681.
14. Lee JH, Huh YM, Jun YW, Seo JW, Jang JT, Song HT, et al. Artificially engineered magnetic nanoparticles for ultra-sensitive molecular imaging. Nat Med. 2007; 13: 95-9.
15. Wang S, Lin J, Wang Z, Zhou Z, Bai R, Lu N, et al. Core-Satellite Polydopamine-Gadolinium-Metallofullerene Nanotheranostics for Multimodal Imaging Guided Combination Cancer Therapy. Adv Mater. 2017; 29: 1701013.
16. Lin J, Wang M, Hu H, Yang X, Wen B, Wang Z, et al. Multimodal-Imaging-Guided Cancer Phototherapy by Versatile Biomimetic Theranostics with UV and gamma-Irradiation Protection. Adv Mater. 2016; 28: 3273-9.
17. Zhang L, Sheng D, Wang D, Yao Y, Yang K, Wang Z, et al. Bioinspired Multifunctional Melanin-Based Nanoliposome for Photoacoustic/Magnetic Resonance Imaging-Guided Efficient Photothermal Ablation of Cancer. Theranostics. 2018; 8: 1591-606.
18. Zhang W, Liu L, Chen H, Hu K, Delahunty I, Gao S, et al. Surface impact on nanoparticle-based magnetic resonance imaging contrast agents. Theranostics. 2018; 8: 2521-48.
19. Zhao Y, Meng J, Sheng X, Tian Y. Synthesis of ultrathin MnS shell on ZnS: Mn nanorods by one-step coating and doping for MRI and fluorescent imaging. Adv Opt Mater. 2016; 4: 1115-23.
20. Chen W, Wang X, Zhao B, Zhang R, Xie Z, He Y, et al. CuS-MnS2 nano-flowers for magnetic resonance imaging guided photothermal/photodynamic therapy of ovarian cancer through necroptosis. Nanoscale. 2019; 11: 12983-9.
21. Huang X, Deng G, Han Y, Yang G, Zou R, Zhang Z, et al. Right Cu2- x S@MnS Core-Shell Nanoparticles as a Photo/H2O2-Responsive Platform for Effective Cancer Theranostics. Adv Sci (Weinh). 2019; 6: 1901461.
22. Bennewitz MF, Lobo TL, Nkansah MK, Ulas G, Brudvig GW, Shapiro EM. Biocompatible and pH-sensitive PLGA encapsulated MnO nanocrystals for molecular and cellular MRI. ACS Nano. 2011; 5: 3438-46.
23. Yang G, Xu L, Chao Y, Xu J, Sun X, Wu Y, et al. Hollow MnO2 as a tumor-microenvironment-responsive biodegradable nano-platform for combination therapy favoring antitumor immune responses. Nat Commun. 2017; 8: 902-10.
24. Fan W, Bu W, Shen B, He Q, Cui Z, Liu Y, et al. Intelligent MnO2 nanosheets anchored with upconversion nanoprobes for concurrent pH-/H2O2-responsive UCL imaging and oxygen-elevated synergetic therapy. Adv Mater. 2015; 27: 4155-61.
25. Zhang C, Chen W-H, Liu L-H, Qiu W-X, Yu W-Y, Zhang X-Z. An O2 Self-Supplementing and Reactive-Oxygen-Species-Circulating Amplified Nanoplatform via H2O/H2O2 Splitting for Tumor Imaging and Photodynamic Therapy. Adv Funct Mater. 2017; 27: 1700626.
26. He T, Xu H, Zhang Y, Yi S, Cui R, Xing S, et al. Glucose Oxidase-Instructed Traceable Self-Oxygenation/Hyperthermia Dually Enhanced Cancer Starvation Therapy. 2020: 10.7150/thno.40439.
27. Yang R, Hou M, Gao Y, Lu S, Zhang L, Xu Z, et al. Biomineralization-inspired Crystallization of Manganese Oxide on Silk Fibroin Nanoparticles for in vivo MR/fluorescence Imaging-assisted Tri-modal Therapy of Cancer. Theranostics. 2019; 9: 6314-33.
28. Cheng Y, Zhang S, Kang N, Huang J, Lv X, Wen K, et al. Polydopamine-coated manganese carbonate nanoparticles for amplified magnetic resonance imaging-guided photothermal therapy. ACS Appl Mater Inter. 2017; 9: 19296-306.
29. Chu C, Lin H, Liu H, Wang X, Wang J, Zhang P, et al. Tumor Microenvironment-Triggered Supramolecular System as an In Situ Nanotheranostic Generator for Cancer Phototherapy. Adv Mater. 2017; 29: 1605928.
30. Liu R, Jing L, Peng D, Li Y, Tian J, Dai Z. Manganese (II) Chelate Functionalized Copper Sulfide Nanoparticles for Efficient Magnetic Resonance/Photoacoustic Dual-Modal Imaging Guided Photothermal Therapy. Theranostics. 2015; 5: 1144-53.
31. Ferretti AM, Mondini S, Ponti A. Manganese Sulfide (MnS) Nanocrystals: Synthesis, Properties, and Applications. 2016.
32. Meng J, Zhao Y, Li Z, Wang L, Tian Y. Phase transfer preparation of ultrasmall MnS nanocrystals with a high performance MRI contrast agent. RSC Adv. 2016; 6: 6878-87.
33. Tang Z, Liu Y, He M, Bu W. Chemodynamic Therapy: Tumour Microenvironment-Mediated Fenton and Fenton-like Reactions. Angew Chem Int Ed Engl. 2019; 58: 946-56.
34. Lyu Y, Tian J, Li J, Chen P, Pu K. Semiconducting Polymer Nanobiocatalysts for Photoactivation of Intracellular Redox Reactions. Angew Chem Int Ed. 2018; 57: 13484-8.
35. Hu D, Chen L, Qu Y, Peng J, Chu B, Shi K, et al. Oxygen-generating Hybrid Polymeric Nanoparticles with Encapsulated Doxorubicin and Chlorin e6 for Trimodal Imaging-Guided Combined Chemo-Photodynamic Therapy. Theranostics. 2018; 8: 1558-74.
36. Lin L-S, Song J, Song L, Ke K, Liu Y, Zhou Z, et al. Simultaneous fenton-like ion delivery and glutathione depletion by MnO2 -based nanoagent to enhance chemodynamic therapy. Angew Chem Int Ed Engl. 2018; 57: 4902-6.
37. Jones D. Gas therapy. Nature. 1996; 383: 676-.
38. Basudhar D, Ridnour LA, Cheng R, Kesarwala AH, Heinecke J, Wink DA. Biological signaling by small inorganic molecules. Coord Chem Rev. 2016; 306: 708-23.

39. Powell CR, Dillon KM, Wang Y, Carrazzone RJ, Matson JB. A Persulfide Donor Responsive to Reactive Oxygen Species: Insights into Reactivity and Therapeutic Potential. Angew Chem Int Ed Engl. 2018; 57: 6324-8.
40. An L, Wang X, Rui X, Lin J, Yang H, Tian Q, et al. The in situ sulfidation of Cu2O by endogenous H2S for colon cancer theranostics. Angew Chem Int Ed. 2018; 57: 15782-6.
41. Wang Y, Huang X, Tang Y, Zou J, Wang P, Zhang Y, et al. A light-induced nitric oxide controllable release nano-platform based on diketopyrrolopyrrole derivatives for pH-responsive photodynamic/photothermal synergistic cancer therapy. Chem Sci. 2018; 9: 8103-9.
42. Fan W, Lu N, Huang P, Liu Y, Yang Z, Wang S, et al. Glucose-responsive sequential generation of hydrogen peroxide and nitric oxide for synergistic cancer starving-like/gas therapy. Angew Chem Int Ed Engl. 2017; 56: 1229-33.
43. Lin WC, Huang CC, Lin SJ, Li MJ, Chang Y, Lin YJ, et al. In situ depot comprising phase-change materials that can sustainably release a gasotransmitter H2S to treat diabetic wounds. Biomaterials. 2017; 145: 1-8.
44. Szabo C. Hydrogen sulphide and its therapeutic potential. Nat Rev Drug Discov. 2007; 6: 917-35.
45. Ciocci M, Iorio E, Carotenuto F, Khashoggi HA, Nanni F, Melino S. H2S-releasing nanoemulsions: a new formulation to inhibit tumor cells proliferation and improve tissue repair. Oncotarget. 2016; 7: 84338-58.
46. Li L, Whiteman M, Guan YY, Neo KL, Cheng Y, Lee SW, et al. Characterization of a novel, water-soluble hydrogen sulfide-releasing molecule (GYY4137): new insights into the biology of hydrogen sulfide. Circulation. 2008; 117: 2351-60.
47. Moloto N, Moloto MJ, Kalenga M, Govindraju S, Airo M. Synthesis and characterization of MnS and MnSe nanoparticles: morphology, optical and magnetic properties. Opt Mater. 2013; 36: 31-5.
48. Ke K, Yang W, Xie X, Liu R, Wang L-L, Lin W-W, et al. Copper manganese sulfide nanoplates: a new two-dimensional theranostic nanoplatform for MRI/MSOT dual-modal imaging-guided photothermal therapy in the second near-infrared window. Theranostics. 2017; 7: 4763-76.
49. Huo M, Wang L, Chen Y, Shi J. Tumor-selective catalytic nanomedicine by nanocatalyst delivery. Nat Commun. 2017; 8: 357-69.
50. Peng B, Chen W, Liu C, Rosser EW, Pacheco A, Zhao Y, et al. Fluorescent probes based on nucleophilic substitution-cyclization for hydrogen sulfide detection and bioimaging. Chemistry. 2014; 20: 1010-6.